



Evidence for the Existence of a Secondary Pathway for Fibril Growth during the Aggregation of Tau

Gayathri Ramachandran and Jayant B. Udgaonkar*

National Centre for Biological Sciences, Tata Institute of Fundamental Research, Bangalore 560065, India

Received 11 November 2011;
received in revised form
2 January 2012;
accepted 5 January 2012
Available online
17 January 2012

Edited by S. Radford

Keywords:

tau;
heparin;
amyloid fibril;
protein aggregation;
neurodegeneration

The mechanism of amyloid fibril formation by proteins has been classically described by the nucleation-dependent polymerization (NDP) model, which makes certain predictions regarding the kinetics of fibrillation. All proteins whose aggregation conforms to the NDP model display a t^2 time dependence for their initial reaction profile. However, there are proteins whose aggregation reactions have kinetic signatures of a flat lag phase followed by an exponential rise in fibril mass, which does not conform to the NDP model. Amyloid fibril formation by tau, a microtubule-associated protein whose aggregation to form neurofibrillary tangles is implicated in Alzheimer's disease and other tauopathies, in the presence of inducers such as heparin and fatty acid micelles, has always been traditionally described by a ligand-induced NDP model. In this study, the existence of a secondary pathway for fibril growth during the aggregation of the functional, repeat domain of tau in the presence of heparin has been established. Both kinetic and accessory evidence are provided for the existence of this pathway, which is shown to augment the primary homogeneous nucleation pathway. From the kinetic data, the main secondary pathway that is operative appears to be fibril fragmentation but other pathways such as branching or secondary nucleation may also be operative.

© 2012 Elsevier Ltd. All rights reserved.

Introduction

The assembly of misfolded forms of soluble and functional proteins or peptides into ordered structures called amyloid fibrils is a process associated with numerous disease conditions, including, prominently, neurodegeneration.¹ Understanding the mechanism of amyloid fibril formation and identifying the toxic aggregates on the fibrillation pathway are, consequently, intensive fields of study.^{2–4} Amyloid fibril formation reactions are usually describable either by isodesmic or by nucleation-dependent polymerization (NDP) models.^{5–8} The aggregation reactions leading to fibril formation

appear complex because oligomers of different sizes and structures are invariably observed to accumulate transiently during the time course of fibril formation.^{9–11} The first step towards delineating the heterogeneity of a fibril formation reaction is to determine whether the isodesmic model or the NDP model is applicable, or whether aspects of both are.⁴ Only then can the complexity of fibrillogenesis be dissected out.

The NDP model or generalized versions of the model have been successfully used to describe the kinetics of self-assembly of proteins such as actin^{12–14} and tubulin.¹⁵ It has also been used to describe the formation of amyloid fibrils by many proteins, although only in a few cases have all three kinetic criteria defining an NDP model^{4,16} been explicitly shown to be met.^{17,18} The NDP model assumes that the nucleus is an oligomer in a highly unfavorable equilibrium with the monomer and that the rate-limiting step in fibrillation is thus the formation of the nucleus, the aggregate with the highest free energy

*Corresponding author. E-mail address:

jayant@ncbs.res.in.

Abbreviations used: NDP, nucleation-dependent polymerization; ThT, thioflavin T; AFM, atomic force microscopy.

and the lowest abundance on the complex energy landscape of aggregation. This model also predicts a strong dependence of the rate of the aggregation reaction on protein concentration, wherein the order of the dependence is related to the nucleus size. Several amyloid fibril-forming proteins display, however, only weak concentration dependences for aggregation,^{19–23} suggesting that the critical nucleus is either monomeric or a very small oligomer. Moreover, several aggregating protein systems display a high apparent cooperativity of conversion,^{22,24} more than that expected from a simple NDP model. These results are not explained satisfactorily by the canonical homogeneous nucleation pathway of an NDP model.

The existence of a high apparent cooperativity of conversion, reflected in kinetic reaction profiles in the form of a flat lag phase and a subsequent steep, exponential increase in polymer mass, was first described for the gelation of sickle cell hemoglobin.^{25,26} Such a kinetic profile, reflecting more cooperativity than that expected from simple NDP, has subsequently been reported for several amyloid protein systems including amylin,²⁷ yeast and mammalian prion protein,^{28,29} insulin,³⁰ glucagon,³¹ and β_2 -microglobulin.³² In all such systems, a secondary polymer-dependent pathway for growth, in addition to the primary nucleation pathway, has been invoked to explain the kinetics. The secondary pathway can be of three main kinds: fragmentation, lateral growth/branching, and secondary/heterogeneous nucleation.⁶ Several models have been formulated to encapsulate the effects of these processes,^{27–29,32,33} and indirect evidence from imaging^{34–36} and seeding experiments^{31,34} has been presented for the occurrence of each of these processes as well. Secondary pathways are important to study because they may have important roles in disease progression by modulating either toxicity^{32,37} of structures formed or infective capacity^{28,38,39} in the case of the prions.

One of the simplest models describing the behavior of a homogeneous nucleation pathway when augmented by a secondary pathway for polymer growth is that proposed by Bishop and Ferrone.⁴⁰ The minimalistic strength of this model lies in its ability to describe all three secondary processes by a single parameter that depends linearly on the concentration of polymerized monomers, which allows the initial kinetic data to be analyzed without any other assumptions. The model also further allows one to extract information about homogeneous nucleation parameters irrespective of the nature of the secondary pathway. Nevertheless, although elegant in its simplicity, this model has so far not been fully applied in the analysis of amyloid fibril formation reactions that are not describable by a simple homogeneous nucleation pathway (NDP) model.

In this study, the existence of a secondary pathway for fibril growth during the aggregation of the microtubule-associated protein tau⁴¹ into amyloid fibrils has been established by careful analysis of the kinetic data. Tau is known to aggregate and form neurofibrillary tangles in Alzheimer's disease as well as in a wide range of other tauopathies.^{42–44} In solution, tau exists as a random coil, and hence belongs to the class of intrinsically disordered proteins.^{45,46} The aggregation of tau *in vitro* is most commonly induced by polyanions such as heparin⁴⁷ or fatty acid and anionic micelles.^{48,49} Studies of the mechanism of tau aggregation are often performed with the microtubule-binding repeat domain of tau⁵⁰ since it has been shown to be a constituent of the amyloid fibril core^{51,52} and its fibrillation time scale is more feasible for study.^{53,54} The amyloid fibril formation mechanism has been described in previous work as ligand-induced NDP,^{53,55–57} but the existence of a secondary pathway for fibril growth has not so far been established. In this work, both kinetic and other evidence are provided for the existence of such pathways during the aggregation of the four-repeat domain of tau in the presence of heparin. From the kinetic data, analyzed quantitatively according to the model incorporating both primary nucleation and secondary pathways for fibril growth,⁴⁰ it appears that the dominant secondary pathway that is operative is fibril fragmentation, although other processes such as branching or secondary nucleation may also contribute to fibril growth.

Results

Amyloid fibril formation by tau-K18 appears to occur by an NDP mechanism

The four-repeat domain of tau (tau-K18) aggregates in the presence of heparin to form amyloid fibrils as seen by an increase in thioflavin T (ThT) fluorescence (Figs. 1 and 2) and by atomic force microscopy (AFM) (Fig. 3). In this quantitative study of amyloid fibril formation by tau-K18, it was necessary to first establish that the kinetic data are highly reproducible. It was especially important to do so because variations have been found to be typically very large for the kinetic traces of amyloid assembly by many other proteins. Figure 1 shows that the typical spread in the data for the aggregation of tau-K18 is small, because of the careful handling of the protein and the aggregation reactions (see [Materials and Methods](#)).

The aggregation reaction shows sigmoidal kinetics, with a distinct lag phase (Fig. 2a). The lag phase has a strong dependence on protein concentration (Fig. 2a and b), shortening with an increase in protein

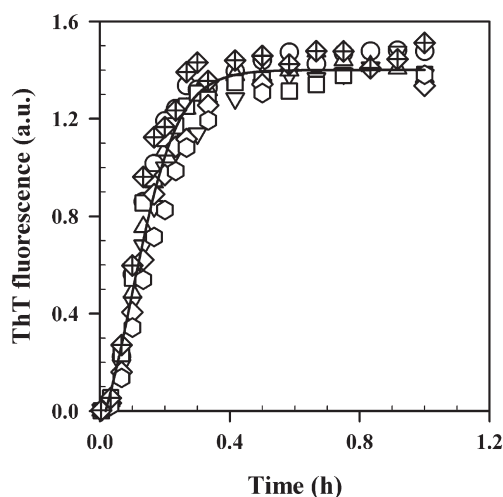


Fig. 1. Reproducibility in the kinetics of formation of amyloid fibrils by tau-K18. ThT fluorescence-monitored kinetics of fibril formation by 50 μM tau-K18 in the presence of 37.5 μM heparin in 25 mM Tris buffer, 50 mM NaCl, and 1 mM DTT (pH 7) at 37 $^{\circ}\text{C}$ are shown. The different symbols represent seven replicates of the data from seven independent experiments, carried out across three different protein preparations. The continuous line through the data points is a global, least-squares fit to Eq. (1).

concentration (Fig. 2b), so that at very high concentrations, the sigmoidal nature of the kinetics appears weaker (Fig. 2a). An analysis, according to Eq. (2), of the protein concentration dependence of the time t_{50} , the time taken to complete 50% of the reaction,^{58,59} provides a value of 3 for the nucleus size (Fig. 2b), but a similar analysis of the protein concentration dependence of the duration of the lag phase¹² provides a slightly higher value of 4 for the nucleus size (Fig. 2b, inset). It should be noted that the nucleus is defined here as the least stable oligomeric intermediate on the aggregation pathway and corresponds to the largest oligomer that remains in equilibrium with the monomer.^{12,58,60} The size of the nucleus defined in this way is one protein unit (monomer) smaller than a nucleus defined, alternatively, as the first stable intermediate^{25,26,61,62} on the pathway of homogeneous nucleation.

Seeding with 10% unsonicated seed was seen to shorten the lag phase but not abolish it (Fig. 2c). Also, the fibrillation process was seen to be characterized by a critical concentration (Fig. 2d). Linear regression analysis of the amplitude of light scattering at 800 nm and of the amount of water-insoluble, denaturant-soluble sediment formed at different protein concentrations provides a value of $3.5 \pm 1.6 \mu\text{M}$ for the critical concentration (Fig. 2d). Since the errors in the determination of the critical concentration are large, the equilibrium monomer concentrations at a time corresponding to three

times the t_{50} ($3t_{50}$) of ThT fluorescence-monitored kinetics for 25, 50, and 100 μM reactions were determined using an ultracentrifugation-based sedimentation assay and were found to be $1.5 \pm 0.3 \mu\text{M}$. At protein concentrations of 1, 2, and 3 μM , fibril formation could not be detected by measurement of ThT fluorescence, even at 100 h of aggregation, while fibril formation by 5 μM protein was detectable. In view of these results, the critical concentration c_s (see Materials and Methods) appears to be about 3 μM .

The kinetics of aggregation of tau-K18 appears therefore to meet all three criteria characteristic of an NDP mechanism, namely, sigmoidal kinetics with an initial lag phase, shortening of the lag phase by the addition of preformed nucleus (seed), and a critical concentration below which aggregation does not occur.^{4,16} This result is in accordance with previous results, which also suggested that tau aggregates *via* an NDP mechanism.^{53,55–57}

ThT fluorescence was chosen as the spectroscopic probe to study the kinetics of aggregation over a 10-fold range of protein concentrations, as the ThT fluorescence-monitored kinetics were highly reproducible as seen by the small spread in the data (Figs. 1 and 2). Other spectroscopic probes including light scattering at 800 nm and a sedimentation assay were also utilized to confirm that the extent of amyloid fibril formation, as measured by ThT fluorescence, was linear with respect to protein concentration over the entire range studied (Fig. 2d). Thus, ThT binding is confirmed to be a reliable, quantitative measure of the amount of fibrils formed.^{63–66} Importantly, the observation that the ThT fluorescence probe chosen to monitor aggregation kinetics has a linear dependence on monomer concentration (Fig. 2d) is important in the context of quantitative modeling of the ThT fluorescence-monitored kinetic curves of aggregation. In particular, since both ThT fluorescence and the amount of water-insoluble, denaturant-soluble sediment scale together with protein concentration (Fig. 2d), it can be assumed that aggregate evolution monitored by ThT fluorescence accurately parallels monomer loss.

Amyloid fibrils formed at different protein concentrations have similar morphologies

AFM images of fibrils formed at time $3t_{50}$ of the ThT fluorescence-monitored kinetics, at three different protein concentrations (10, 25, and 100 μM) that span the entire range of protein concentrations examined in this study, reveal no significant differences in fibril morphology (Fig. 3). The fibrils formed at all concentrations have similar lengths and heights, on average. The fibrils appear to be straight filaments and, as described earlier,⁶⁷ have heights of ~ 8 nm and ~ 12 nm at the valley and peak of fibril height cross sections, respectively (data not

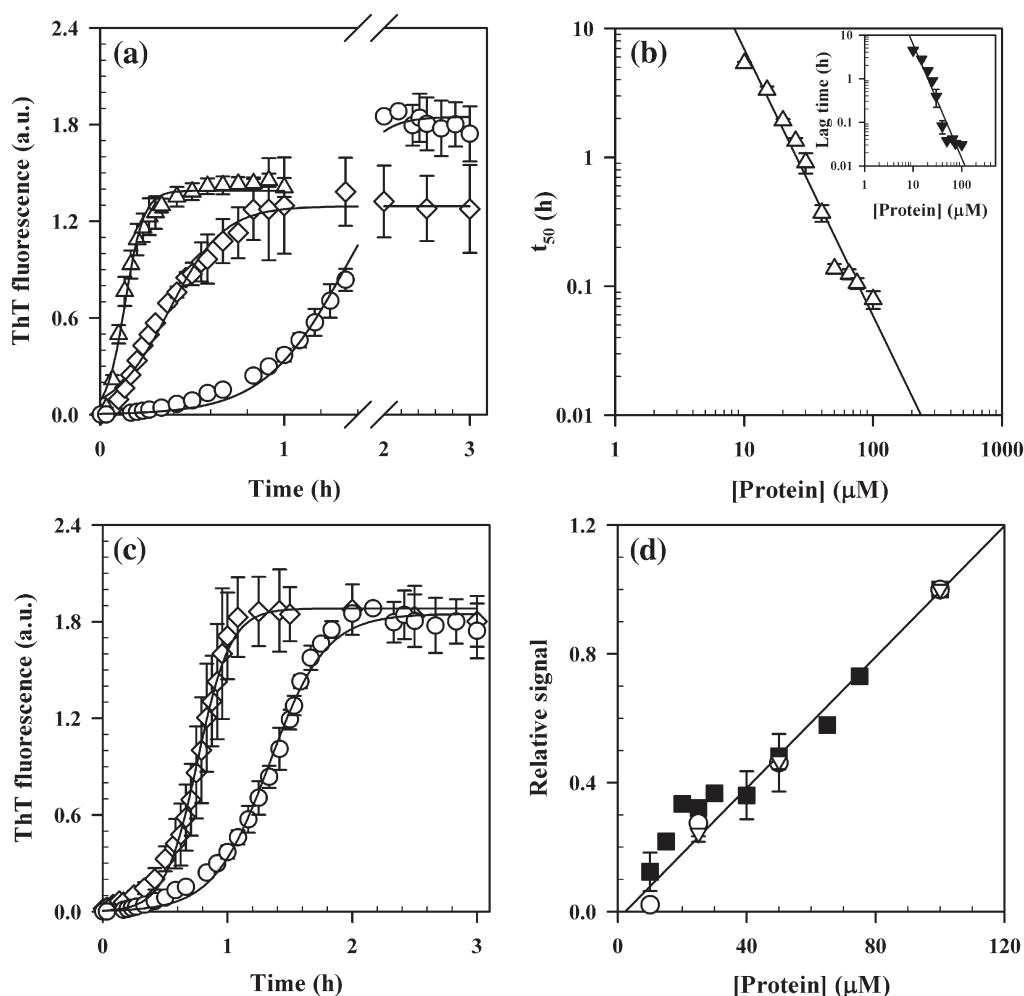


Fig. 2. Kinetics of formation of amyloid fibrils by tau-K18 in the presence of 37.5 μM heparin at 37 $^{\circ}\text{C}$. (a) ThT fluorescence-monitored kinetics in 25 mM Tris buffer, 50 mM NaCl, and 1 mM DTT (pH 7) of 25 μM (O), 40 μM (\diamond), and 50 μM (Δ) tau-K18. The continuous lines through the data points are least-squares fits to Eq. (1). The data shown for each kinetic curve were obtained by assaying the ThT fluorescence of 1 μM aggregate at every time point depicted. The kinetic curves are hence directly comparable, and there is no need to normalize them for their initial monomer concentrations. (b) A plot of the t_{50} values of the ThT fluorescence-monitored kinetic curves, against protein concentration. The straight line through the data points is a least-squares fit to Eq. (2); the slope $[(i+1)/2]$ of 2.07 ± 0.06 yields a value of ~ 3 for i . The inset shows a plot of the lag time of ThT fluorescence-monitored kinetics against protein concentration. The straight line through the data points is a least-squares fit to Eq. (2), and the slope of 2.60 ± 0.08 yields a value of ~ 4 for i . (c) Effect of seeding. ThT fluorescence-monitored kinetics of 25 μM tau-K18 in the presence of 37.5 μM heparin were determined in the absence (O) and presence (\diamond) of 10% (v/v) unsonicated seed. The continuous line through the data points is a least-squares fit to Eq. (1). (d) The extent of amyloid fibril formation at the end of the reaction is linear with respect to protein concentration when monitored by ThT fluorescence (\blacksquare), light scattering (O), and a sedimentation assay (∇). The data points correspond to the amplitude of signal change measured at a time corresponding to $3t_{50}$ of the ThT fluorescence-monitored kinetics. The data have been normalized to their respective signals obtained at 100 μM tau-K18. The straight line is a least-squares fit to all of the data. The critical concentration calculated by linear regression analysis of the light scattering and sedimentation assay data sets is $3.5 \pm 1.6 \mu\text{M}$. For all the plots, the error bars represent the spread in the data calculated from two or more independent experiments carried out across different protein preparations.

shown). At higher protein concentrations (100 μM), unlike at the lower concentrations, the fibrils tend to form clumps and fibril fragments are more apparent (Fig. 3c). In addition, the AFM images provide approximate visual evidence for a scaling in the final

amount of fibril polymer formed, with starting protein concentration (Fig. 3).

One of the interesting fibril morphologies observed in this study were coiled spring-like fibrils seen at the end of the aggregation reaction (Fig. 3b,

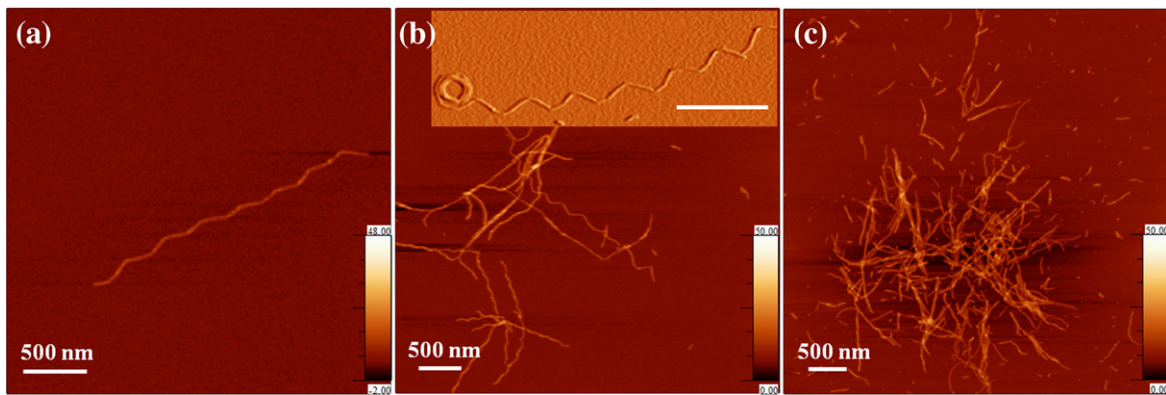


Fig. 3. Fibril morphology. AFM images in the topography format, obtained at times $3t_{50}$ of ThT fluorescence-monitored kinetics of aggregation of (a) 10 μM , (b) 25 μM , and (c) 100 μM of tau-K18 aggregation in the presence of 37.5 μM heparin. The inset in (b) corresponds to an image in the amplitude format of a coiled spring-like fibril seen in the same condition. The scale bar for all images represents 500 nm. The Z height for the images corresponds to 50 nm, as shown in the color scale.

inset). Several wavy fibrils were seen, for the aggregation of both 10 μM and 25 μM tau-K18 (Fig. 3a and b), and the observation of the coiled spring-like fibril suggests that these wavy fibrils could be fibrils that have become completely uncoiled. This hypothesis was confirmed by measuring the circumference of the coiled spring-like fibril (circumference = 250 nm) and finding that it equaled the length of one turn (~ 250 nm) of the wavy fibril that emerged from the coiled fibril (Fig. 3b, inset).

The shape of the aggregation curve depends on the initial monomer concentration

One of the intriguing observations made in this study is that the kinetic profile of aggregation as typified, for example, by the shape of the lag phase has a dependence on the initial monomer concentration. At the three lowest concentrations studied, 10, 15 and 20 μM , a flat lag phase is succeeded by a steep exponential increase in fibril mass, while at all higher concentrations (25–100 μM), the lag phase and subsequent fibril growth are better described by a t^2 function. Figure 4a illustrates this pattern for the aggregation of 10, 20, 25, and 100 μM tau-K18. This difference in kinetic profiles is more clearly apparent in a double-log plot of fractional change *versus* time (Fig. 4b). At the lowest concentrations (10 and 20 μM), the line drawn through the data points that encompass 1–80% of the fractional change is steeper than an equivalent line drawn for the higher concentrations (25 and 100 μM) (Fig. 4b). The slope of the line has a value of 5.2 ± 0.7 for the three lowest concentrations, while at all higher concentrations studied, the slope of the line has a value of 2.2 ± 0.2 . Not surprisingly then, when the time axis is also normalized by making a fractional change *versus*

t/t_{50} plot,¹⁵ two categories of data collapse are observed (Fig. 4c), indicating two types of aggregation behavior. The data for the three lowest concentrations (10, 15, and 20 μM) were found to collapse together, while the rest of the data collapse in a separate group (Fig. 4c).

In order to better understand the nature of the difference in kinetic profiles, the initial 10% of each kinetic curve was fit to both an $\exp t$ function and a t^2 function. The initial parts of the kinetic curves obtained at higher protein concentrations (25–100 μM) were found to fit very well to a t^2 dependence. Figure 5c and d illustrates this point for the initial parts of the aggregation curves of 25 and 75 μM tau-K18. On the other hand, the initial parts of the kinetic curves obtained at lower protein concentrations (10–20 μM) were found to fit very well to an $\exp t$ function but not to a t^2 function. Figure 5a and b illustrates this point for the initial parts of the aggregation curves of 10 and 20 μM tau-K18.

The kinetic data at all protein concentrations are best explained by a model that assumes that homogeneous nucleation is augmented by a secondary pathway for fibril growth

The aggregation data suggest that the aggregation mechanism is more complex at lower protein concentrations, because the initial parts of the kinetic curves belonging to the group of lower protein concentrations require to be described by an $\exp t$ time dependence, while those belonging to the group of higher protein concentrations are describable by a simpler t^2 time dependence. While the t^2 time dependence has been deemed to be one of the key signatures of a homogeneous nucleation mechanism,^{5,6} an $\exp t$ time dependence is often

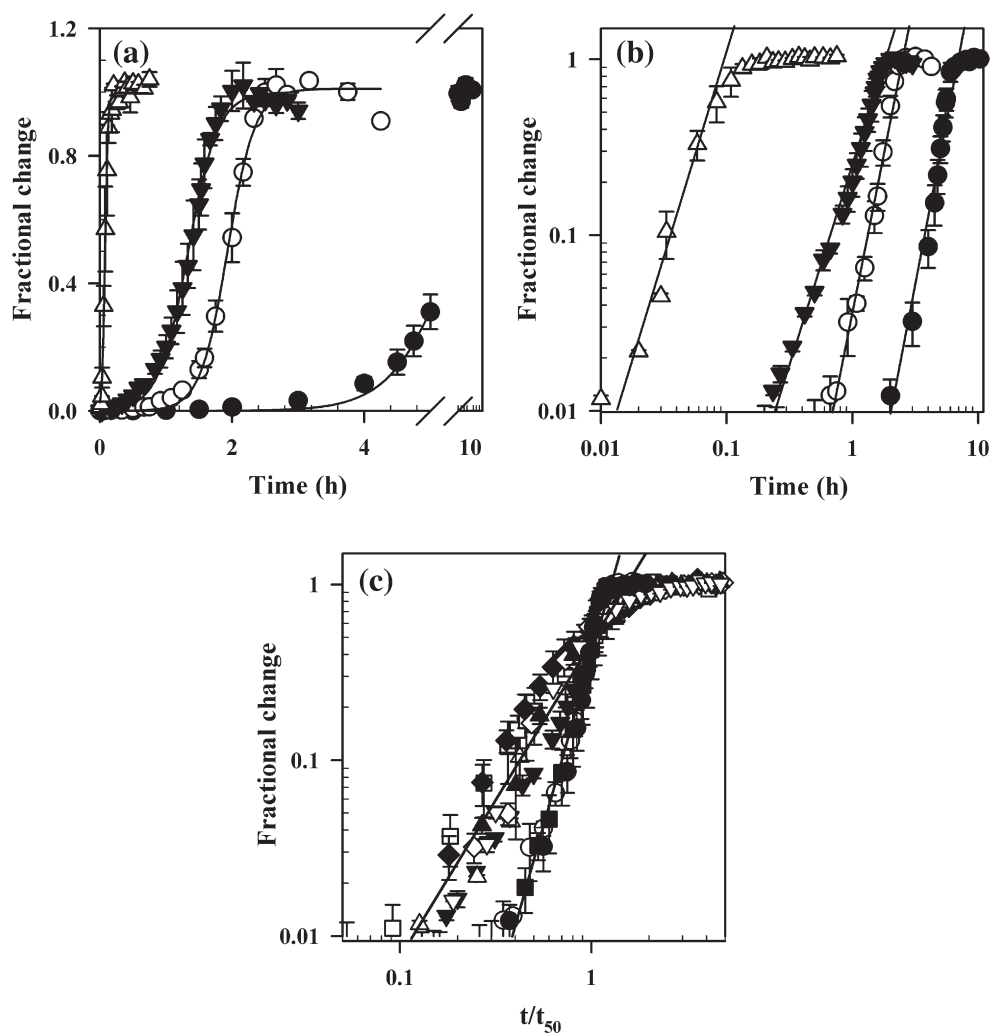


Fig. 4. Kinetic profiles of aggregation. (a) Kinetic curves of aggregation showing the fractional change in ThT fluorescence *versus* time of aggregation at different protein concentrations in the presence of 37.5 μM heparin. The continuous lines through the data points are least-squares fits to Eq. (1). (b) The same data as in (a), but plotted using double-log axis. The continuous lines through the data points were drawn by inspection. (c) A fractional change *versus* t/t_{50} plot showing the collapse of the entire data set into two separate groups. The continuous lines through the data points were drawn by inspection. In the three panels, data are shown for the following protein concentrations: 10 μM (\bullet), 15 μM (\blacksquare), 20 μM (\circ), 25 μM (\blacktriangledown), 30 μM (\square), 40 μM (\blacklozenge), 50 μM (\diamond), 65 μM (\blacktriangle), 75 μM (∇), and 100 μM (\triangle). For all the plots, the error bars represent the spread in the data calculated from two or more independent experiments and across different protein preparations.

cited as evidence for a secondary pathway for aggregate growth being operative.²⁴ When a homogeneous nucleation pathway is augmented by secondary polymer-growth pathways, it has been shown by Bishop and Ferrone, using a linear perturbation approach, that the initial part of the kinetic data should be describable by a cosh t time dependence (see [Materials and Methods](#)).⁴⁰ Indeed, it is found (insets to [Fig. 5](#)) that the initial increase in the concentration of polymerized monomer, Δ , is well described by the equation $\Delta = A (\cosh Bt - 1)$ [Eq. (8)] for aggregation at all protein concentra-

tions. It is important to note that the extended Bishop and Ferrone NDP model makes certain critical assumptions. These include the assumptions that (a) monomers do not possess any internal structure or undergo any structural changes; (b) pre-nuclear oligomeric aggregates that are in equilibrium with the monomer have concentrations that are negligible when compared with the free monomer or the polymerized monomers; (c) the nucleus size is fixed and does not change as a function of protein concentration; and (d) the concentration of polymerized monomer, Δ ,

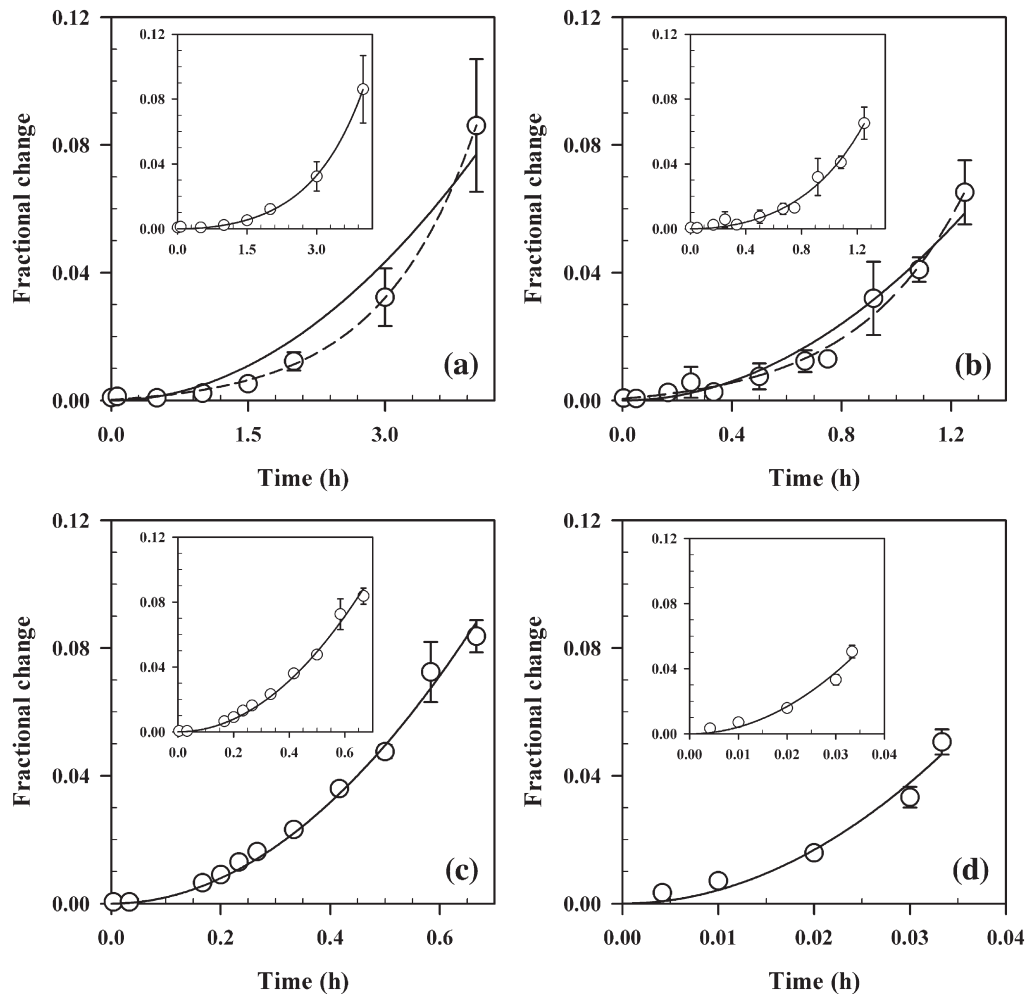


Fig. 5. Initial time courses of aggregation. The initial 10% of the ThT fluorescence-monitored kinetic curves of aggregation of (a) 10 μM , (b) 20 μM , (c) 25 μM , and (d) 75 μM tau-K18 in the presence of 37.5 μM heparin. In all the plots, the broken line is a least-squares fit to an exponential equation, $\Delta = ae^{kt}$, and the black continuous line is a least-squares fit to a quadratic equation, $\Delta = at^2$. The insets in all four panels show that the data fit well to Eq. (8); the continuous line through the data points is a least-squares fit to Eq. (8). In all the plots, the error bars represent the spread in the data calculated from two or more independent experiments carried out across different protein preparations.

changes by monomer addition or loss at the polymer ends and this process is independent of length for long polymers. Further analysis of the kinetic data was carried out on the basis of these assumptions.

The homogeneous nucleus for tau-K18 aggregation appears to be a trimer

The values of the parameters A and B were obtained at all protein concentrations (Fig. 6a and b) by fitting the initial increase in the concentration of polymerized monomer (Δ) to Eq. (8). The values of A and B were then used in Eq. (11), to determine the size of the equilibrium nucleus (the largest unstable aggregate that remains in equilibrium with the

monomer) (Fig. 6c). This analysis yields a trimer for the equilibrium nucleus size (Fig. 6c). It should be noted that the quantity B^2A in Eq. (11) has the same form in the absence and presence of a secondary pathway;⁶ hence, the presence of a secondary pathway for fibril growth does not affect the determination of the size of the equilibrium nucleus for homogeneous nucleation.

The stoichiometry of tau bound to heparin in the rate-limiting steps of aggregation⁶⁸ can be determined from the hyperbolic dependence of the extent of fibril formation on heparin concentration. This dependence yields only the stoichiometry of binding⁶⁸ and not the binding constant, because the binding of heparin to tau is tight with a submicromolar dissociation constant.^{57,69,70} The

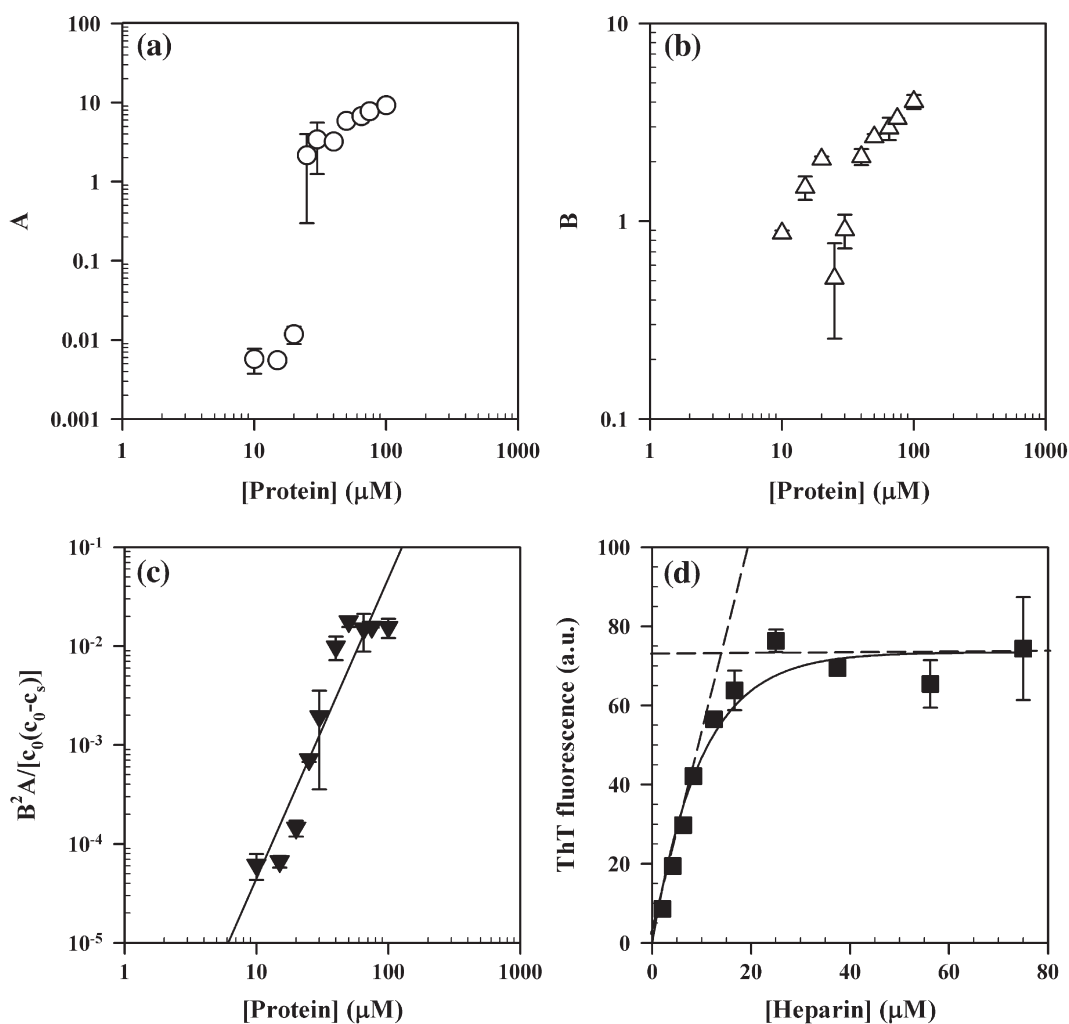


Fig. 6. Determination of homogeneous nucleation parameters for tau-K18 polymerization in the presence of heparin. (a) Dependence of the parameter A on protein concentration. (b) Dependence of the parameter B on protein concentration. (c) Nucleus size determined by analysis based on the NDP model augmented by a secondary polymer-growth pathway, as described in [Materials and Methods](#). The straight line through the data points is a least-square fit. The slope of the plot determined by linear regression analysis equals the nucleus size, i , and is 3.03 ± 0.03 . (d) The amplitude of change in ThT fluorescence plotted against heparin concentration when protein concentration is held constant at $50 \mu\text{M}$. The continuous line through the data points was drawn by inspection. The broken lines are also lines drawn by inspection to aid estimation of stoichiometry. They intersect at a protein-to-heparin molar ratio of $\sim 3:1$. For all the plots, the error bars represent the spread in the data calculated from two or more independent experiments and across different protein preparations.

ThT fluorescence appears to saturate at a protein-to-heparin molar ratio of about 3:1 (Fig. 6d). Since the kinetic role of heparin is restricted mainly to the rate-limiting steps of aggregation,⁵⁷ it is likely that the equilibrium nucleus is composed of three protein molecules held together by one heparin molecule. Future studies will address the important question of whether heparin, in addition to affecting the initial equilibrium between the monomer and the trimeric nucleus, also has roles in modulating growth by both the primary and the secondary pathways.

The nature of the secondary pathway for fibril growth

The values obtained for the parameters A and B at different values of the total monomer protein concentration, c_0 , are used to determine the quantity k_+Q_0 at each protein concentration, using Eq. (12). The nature of the secondary process can then be determined from a plot of $\log k_+Q_0$ versus $\log c_0$ (Fig. 7). When the secondary process is fragmentation, such a plot would have a slope of zero; when the secondary process is lateral growth,

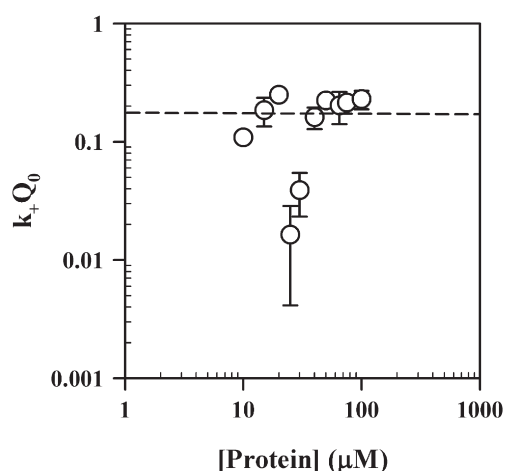


Fig. 7. Determination of the nature of the secondary pathway for fibril growth. The dependence of Q_0 scaled with k_+ on protein concentration, calculated using the values for A and B as well as the nucleus size from Figure 6c, and with the use of Eq. (12), has been plotted. The short broken line drawn by inspection represents what is expected for fragmentation (constant Q_0). Lateral growth/branching corresponds to a slope of unity and would hence be represented by the diagonal of the plot. If the slope of the line exceeds unity, that would be diagnostic of heterogeneous nucleation. The error bars represent the spread in the data calculated from two or more independent experiments and across different protein preparations.

such a plot would have a slope of unity; and when the secondary process is heterogeneous nucleation, the slope would give the heterogeneous nucleus size.⁴⁰ It appears from Fig. 7 that the dominant secondary pathway is fragmentation, but other processes such as lateral growth or secondary nucleation may also be operative.

The addition of sonicated fibrils (seeds) abolishes the lag phase

Figure 8 illustrates the effects of sonicated seed on the abolition of the lag phase during the aggregation of 25 μM tau-K18. As is evident, the addition of even very small amounts of sonicated seed (0.1%) (v/v) begins to shorten the lag phase. The addition of 1% and 10% sonicated seed (v/v) completely abolishes the lag phase and hastens the aggregation process dramatically. This is in contrast to the inability of 10% unsonicated seed (v/v) to completely abolish the lag phase (Fig. 2c).

Fibril clumps and fragments of fibrils are seen during the lag phase of aggregation

Clumps of fibrils are seen very early in the aggregation reaction, at 10, 30, and 55 min of

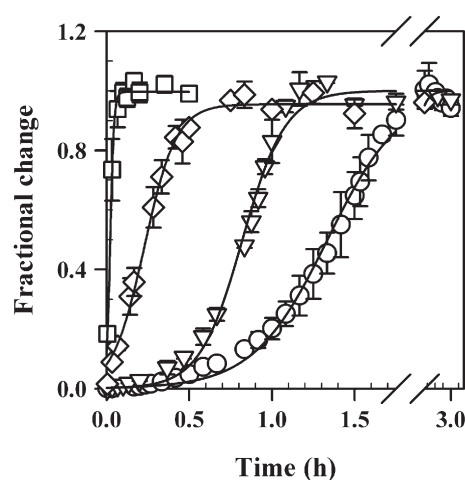


Fig. 8. The effect of sonicated seed on the abolition of the lag phase. ThT fluorescence-monitored kinetics of amyloid fibril formation by 25 μM tau-K18 in the presence of 37.5 μM heparin in the absence (O) and presence of 0.1% (∇), 1.0% (\diamond), and 10% (\square) sonicated seed (v/v). The continuous lines through the data points are least-squares fits to Eq. (1). The error bars represent the spread in the data calculated from two or more independent experiments and across different protein preparations.

aggregation of 25 μM protein, when the lag time of aggregation is ~ 55 min (Figs. 9a–c, insets, and 2b, inset). These clumps are, however, populated sparsely, as is evident from the $90 \times 90 \mu\text{m}$ scans of the mica (Fig. 9a–c, white arrows). In contrast, at the end of the aggregation reaction, the mica surface is covered with amyloid fibrils (Fig. 9d).

To confirm that only a small fraction of the protein molecules form fibrils during the lag phase, we acquired CD spectra at 10, 30, and 55 min of aggregation. No significant change in CD signal at 216 nm was observed (Supplementary Fig. 1). The CD data are also consistent with the low level of ThT binding and fluorescence seen during the lag phase of aggregation (Fig. 4a). A sedimentation assay coupled to ultracentrifugation was performed at 10 min of aggregation, and it was found that monomer protein concentration had changed from 25 μM to 22.5 μM ; thus, 90% of the protein is still monomeric. Hence, it appears that only a small fraction of protein molecules form the clumps of fibrils observed early during the aggregation reaction and that the formation of these clumps is not detectable by either ThT binding or CD.

In order to determine if similar structures are formed in the lag phase of aggregation at other protein concentrations, we acquired AFM images at the time t_{10} of 10 μM and 40 μM tau-K18 aggregation, as determined from ThT fluorescence-monitored kinetics (Figs. 10 and 2b, inset). As is evident, there are discrete, longer fibrils (Fig. 10a) and more fibril fragments (fibrils ≤ 500 nm in length)

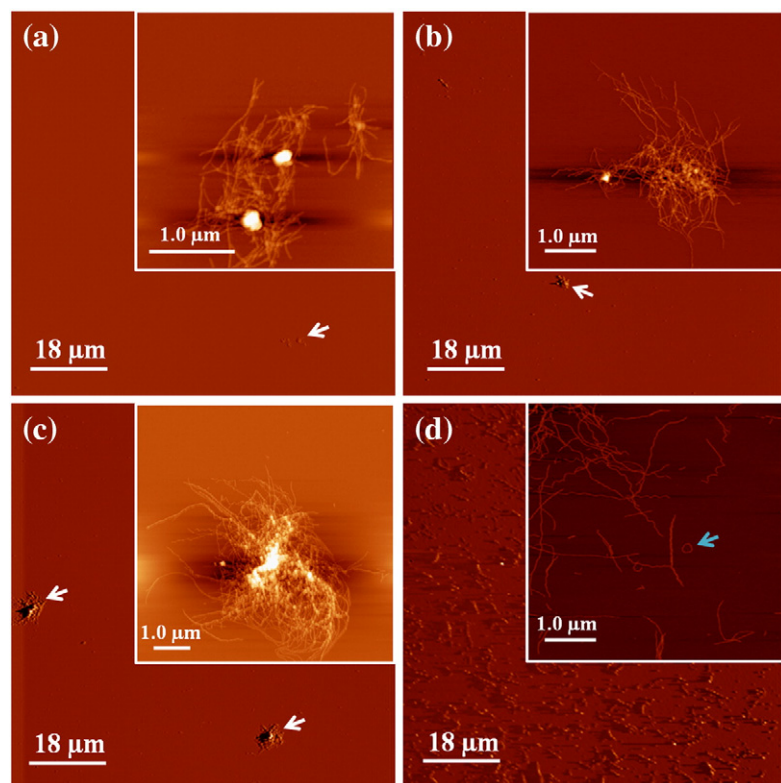


Fig. 9. AFM images of structures formed in the lag phase and at the end of the aggregation reaction of 25 μM tau-K18 in the presence of 37.5 μM heparin. Images were acquired at (a) 10 min, (b) 30 min, (c) 55 min, and (d) 4 h of aggregation. The main images are 90 \times 90 μm scans of the respective time points and are shown in the amplitude format. The insets are images in the topography format. The scale bar for all the insets represents 1.0 μm . The Z height of all the insets corresponds to 150 nm. The white arrows, in the main images of (a), (b), and (c), point to clumps of fibrils. The blue arrow in the inset of (d) points to an annular amyloid fibril.

at the end of the lag phase of 10 μM tau-K18 aggregation when compared with 25 μM protein (Fig. 10b). Also, the longer fibrils appear to have formed large clumps in the case of 25 μM tau-K18 aggregation (Fig. 10b). At 40 μM protein, the clumps of fibrils formed at the end of the lag phase are smaller and are composed of shorter fibrils (Fig.

10c). There is also an increase in the number of fibril fragments (fibrils ≤ 500 nm in length) at the end of the lag phase of 40 μM tau-K18 aggregation when compared with 25 μM (Fig. 10c). In all, the AFM evidence indicates that fibrillar structures are formed in the lag phase, which are likely to play a role in fibril growth by the secondary pathway.

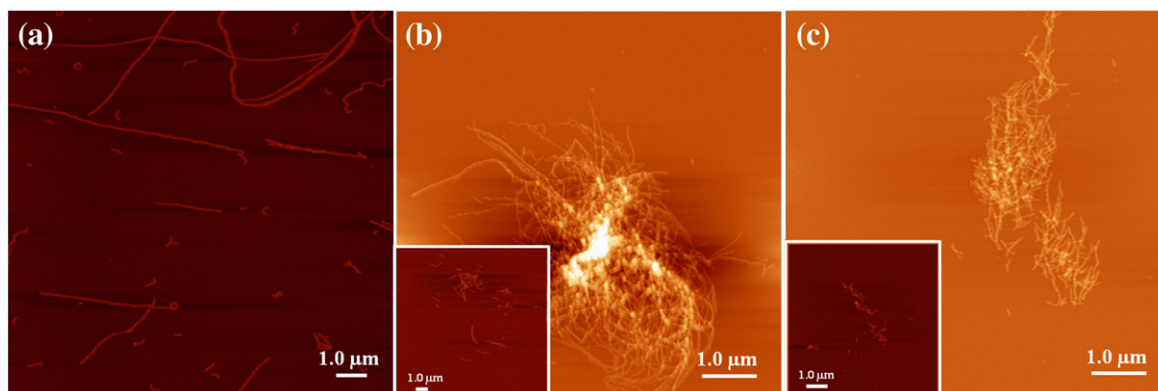


Fig. 10. AFM images of structures formed at the end of the lag phase of ThT fluorescence-monitored aggregation kinetics. Images in the topography format, acquired at time t_{10} of the ThT fluorescence-monitored aggregation kinetics of (a) 10 μM , (b) 25 μM , and (c) 40 μM tau-K18, in the presence of 37.5 μM heparin. In (b) as well as in (c), the inset shows an AFM image of another view of the mica surface; the two AFM images represent views of the mica acquired across protein preparations and have been chosen such that they are representative of the kinds of structures seen in other views. The images were acquired using a large scanner. The scale bar for all images represents 1.0 μm . The Z heights of all images correspond to 150 nm.

Discussion

The NDP model cannot fully explain tau fibrillation

Previous studies of amyloid fibril formation by tau in the presence of heparin^{53,57,70} or other inducers^{55,56,71} had suggested that the aggregation reaction could be described by the NDP model. Indeed, in this study, the kinetics of fibril formation by tau-K18 display the three characteristic features of NDP, namely, an initial lag phase dependent on protein concentration, a critical protein concentration below which aggregation does not occur, and an accelerating effect upon the addition of preformed fibrils (seeds) (Fig. 2). Nevertheless, the basic NDP model incorporating only a primary homogeneous nucleation pathway cannot adequately account for all aspects of the kinetics. These include the following: (1) the observation that the kinetic data at low protein concentrations collapse separately and possess a steeper time dependence (Fig. 4) than the kinetic data acquired at higher protein concentrations (see Results), suggesting that the aggregation mechanism is either changing or becoming more complex with a change in protein concentration (Indeed, the protein concentration dependence of reaction profiles has been shown in previous work²⁷ to be a signature of the existence of a distinct secondary pathway with a reaction order that is different from the primary pathway.); (2) the observation that it is necessary to use an exponential function to describe the initial kinetics at low protein concentrations, while the simpler t^2 function expected for an NDP process^{5,6} is an adequate descriptor at higher protein concentrations (Fig. 5); (3) the observation that the addition of unsonicated preformed fibrils as seeds does not completely abolish the lag phase (Fig. 2c), while sonicated seeds do so at very low seed concentration (Fig. 8); and (4) the observation that a simple NDP-based analysis of the protein concentration dependence of the t_D or t_{10} times [an indication of the duration of the lag phase; see Eq. (1)] yields a slightly larger size for the equilibrium nucleus than does a similar analysis of the t_{50} times (Fig. 2b). Hence, it is clear that tau fibrillation cannot be fully explained by a simple ligand-induced NDP mechanism.

Tau fibrillation is best described by an NDP model augmented by a secondary pathway for fibril growth

To quantitatively account for all aspects of the data at all protein concentrations, we used the mathematical formalism used by Ferrone *et al.* to analyze the aggregation of non-amyloidogenic proteins, to analyze the amyloid fibril formation reaction of tau.^{26,40} This analysis is based on augmenting the

basic homogeneous nucleation pathway of the NDP model with a secondary pathway for polymer growth.⁴⁰ It is found that such an extension to the basic NDP model can adequately describe all aspects of the kinetic data in a quantitative manner. In particular, as expected from the extended model, the initial time course of aggregation is adequately described by the expected cosh t time dependence [Eq. (8)] for fibril formation at all protein concentrations (Fig. 5, insets), and the same size for the homogeneous nucleus is obtained as is from a simple NDP-based analysis of t_{50} times (Figs. 6c and 2b).

The observed cosh t time dependence accounts for the switchover from an exp t time dependence at low protein concentrations to a t^2 time dependence at high protein concentrations. At low protein concentrations, homogeneous nucleation is less probable, and hence, the secondary pathway dominates fibril growth, resulting in the high time dependence of aggregation kinetics (Fig. 4b). At the three lowest protein concentrations, the values obtained for the parameter A [Eq. (9)], which determines the shape of the kinetic curve of aggregation, are small (≤ 0.01) (Fig. 6a), and the values obtained for parameter B [Eq. (10)], which serves as an effective rate constant for nucleation, are ≥ 1 (Fig. 6b). For $Bt > 1$ (t_D or t_{10} is longest for the lowest protein concentrations so that the initial process is observable for long times), the cosh t function reduces to an exp t function ($\Delta = \frac{1}{2}A \exp Bt$); hence, exponential behavior is seen at low protein concentrations. At higher protein concentrations, homogeneous nucleation becomes more favorable and produces a larger fraction of the polymer present than does the secondary pathway, thereby resulting in a reduction of auto-catalysis and consequently a reduction in the observed time dependence of the aggregation kinetics (Fig. 4b). At the higher protein concentrations, the values of A are found to have become larger (> 1) (Fig. 6a), the solution is restricted to small values of Bt ($Bt < 1$), and the cosh t function reduces to a t^2 function ($\Delta = \frac{1}{2}B^2 A t^2$). The intriguing feature of the lower protein concentrations displaying an exponential growth pattern while the higher concentrations display quadratic growth patterns has not been seen for any other amyloid-fibril forming protein but has, however, been observed for the gelation of sickle cell hemoglobin.²⁵

The trimeric size of the equilibrium nucleus

Quantitative analysis of the kinetics suggests that the nucleus is a trimer (see Results). The analysis depends on determination of the product $B^2 A$ (Fig. 6c) whose value was found to remain unchanged even if the value of either A or B was altered slightly from that obtained from the free fit of the kinetic curves to Eq. (8). The nucleus size of a trimer is an important conclusion of the model, but it is important to note that the model makes several

assumptions (see Results) and does not explicitly account for the existence of heparin as a part of the structural nucleus. Hence, this nucleus size should only be considered as a good estimate of the size of the actual ephemeral nucleus. A previous study on heparin-induced fibril formation by an artificially created tau dimer had suggested a larger nucleus size,⁵³ and a study on another repeat domain construct had suggested that the nucleus is a dimer.⁵⁷ In the former case, it is likely that the nucleus size was an overestimate, because it was determined from a kinetic model that attributed the changes in velocity to largely nucleation while ignoring elongation.⁷² In the latter case, the dimer size was based on kinetic simulations to a minimal model, which would work equally well with a trimeric nucleus size determined here using equations [Eqs. (2) and (11)] obtained from an analytical description of the aggregation process.

Two results merit further discussion: (1) the size ($i=3$) for the homogeneous nucleus is different from the size determined from the protein concentration dependence of the lag time (t_D), which yields a value of 4 (Fig. 2b, inset); (2) the dependence of fractional change on t/t_{50} for the three lowest protein concentrations is different from that for the higher protein concentrations (Fig. 4c), but nevertheless, the plot of $\log t_{50}$ versus \log protein concentration (Fig. 2b) appears to be linear over the entire range of protein concentrations. It seems that both results might originate from the operation of the secondary pathway early during the aggregation process. Although the detection of clumps and fragments of fibrils during the lag phase of aggregation supports this hypothesis (see below), these results will need to be understood better in future studies.

The main secondary pathway for fibril growth appears to be fragmentation

There are three general possibilities for the secondary pathway.^{6,40} The first is fragmentation or internal scission, which refers to spontaneous or induced breakage of polymers, thereby generating new ends for growth. The second is branching or lateral non-nucleated growth, and the third is heterogeneous nucleation. The distinction between branching and heterogeneous nucleation is the same as that between isodesmic (downhill) polymerization and NDP—in the former, growth on the surface of an existing polymer does not require the formation of a critical nucleus, while in the latter, secondary growth does not occur until a heterogeneous nucleus forms.⁴⁰ In kinetic terms, the formation of new growth centers from existing fibrils results in positive feedback (auto-catalysis), generating an exponential increase in fibril mass. In this study, the dependence of the quantity k_+Q_0 on protein concentration [Eq. (12)] suggests that the

main secondary pathway for fibril growth is fragmentation (Fig. 7), although other processes such as branching or secondary nucleation may also contribute to growth.

Other evidence for the existence of a secondary pathway for fibril growth

The effects of seeding on aggregation reactions that involve a secondary pathway have been examined in the past.^{22,31–34} For tau aggregation in the presence of heparin, the observation that the lag phase is not completely abolished when the aggregation reaction is seeded with 10% unsonicated seed cannot be attributed to a conformational change being rate limiting, as appears to be the case for amylin fibrillation in the presence of HFIP,²² because an increase in the concentration of heparin results in the lag phase of tau aggregation becoming longer and not shorter. The possibility that the existence of a time lag in seeded kinetics is a reflection of the time taken for critical oligomer formation²² is also unlikely since AFM images of the lag phase of unseeded kinetics show no evidence for the existence of oligomers (Figs. 9 and 10).

Previous work with glucagon had suggested that a lag phase in seeded kinetics is an indicator of the existence of a secondary pathway.³⁴ The model used predicted that seeding a kinetic process that includes a secondary pathway will shorten the lag phase but not affect the growth rate. This seems to be the case when seeding is carried out using 10% unsonicated seed (Fig. 2c). However, when sonicated fibrils are provided as seeds, just 1% seed suffices to completely abolish the lag phase (Fig. 8). Both previous work^{29,31} and this study concur that the main effect of sonication is an increase in fibril ends through fragmentation of preformed fibrils. At even lower concentration of sonicated seed (0.1%), a pattern similar to 10% unsonicated seed kinetics is observed where the lag phase is shortened but the elongation rate is largely unaffected (Figs. 2c and 8). Work with glucagon has also shown that at high seed concentrations, even in the presence of a secondary pathway, the lag phase will be bypassed altogether.^{31,33} This presumably occurs because the addition of larger amounts of seed overcomes both the primary nucleation barrier and the requirement for a certain critical mass of fibrils (formed in unseeded kinetics through the secondary pathway), for fibril growth to begin to dominate.

Imaging studies have provided evidence for fibril-dependent secondary nucleation in the case of insulin³⁶ and amylin,³⁵ and for branching as a secondary pathway for glucagon fibrillation.³⁴ In the case of amylin fibrillation, the indirect observation of fibril formation in the lag phase was taken as evidence for a secondary pathway.²⁷ Similarly, the observation of clumps and fragments of fibrils

during the lag phase of tau fibrillation (Figs. 9 and 10), albeit sparse, suggests that these structures provide a secondary pathway for fibril growth. Moreover, more fibril fragments and smaller clumps composed of shorter fibrils are seen at the end of the lag phase of 10 and 40 μM tau-K18 aggregation as compared to 25 μM tau-K18 (Fig. 10). The observation that fibrils are found in clusters, rather than being randomly strewn, might suggest that the mechanism for fibril growth is branching, but there is no evidence that tau-K18 fibrils are branched. It is possible that the fibril clusters are observed as a consequence of the plating of a group of fibers that had fragmented initially. The visual evidence from AFM thus corroborates the result of the kinetic analysis that the dominant secondary pathway for fibril growth during tau aggregation is fragmentation (Fig. 7). In the future, it will be important to determine if more quantitative criteria can be applied to determine the relative numbers of fibril fragments formed initially as a function of protein concentration. At present, this analysis is difficult to perform since the fragments are not easily distinguishable and form tight clumps (Figs. 9 and 10).

A future focus of this work would be a more detailed investigation of the nature of the secondary pathway. In the case of hemoglobin S gelation, the observation that the lengths of fibers are exponentially distributed, independent of reaction time, throughout the lag phase,⁷³ was taken to suggest a double nucleation model in which heterogeneous nucleation of aggregates along fibers is rate limiting. On the other hand, in the case of tau aggregation induced by the small molecule thiazine red, the average length of tau filaments was found to increase monotonically with time, and this was taken as evidence for the absence of secondary nucleation.⁵⁶ Hence, it will be important to investigate the length distributions of tau fibrils induced by heparin.

Comparison with other proposed tau aggregation mechanisms

In this study, it was possible to establish the existence of a secondary pathway for tau fibrillation, because the very reproducible kinetics (Fig. 1) allowed a quantitative analysis of the concentration dependence of the initial time course of the reaction. Interestingly, however, tau aggregation in the presence of anionic micelles⁷⁴ exhibits a kinetic profile of a flat lag phase followed by an exponential rise that is characteristic of the presence of secondary pathways, but no explicit analysis of these data was carried out. In other studies, the existence of exponential length distributions even at early times of aggregation of tau⁷⁵ was attributed to time-dependent nucleation events,⁷⁶ but again, no attempts to pursue the significance of this elegant observation were made.

An earlier study of tau aggregation in the presence of heparin from this group used a His-tagged four-repeat tau construct (tau4RD) and proposed the existence of an off-pathway intermediate leading to the formation of rod-like protofibrils.⁵⁷ It was postulated that the off-pathway intermediate bound heparin more tightly than the on-pathway intermediate. Experiments with tau-K18 that differs from the earlier construct by the absence of two heparin-binding sites—an HK motif and the 6 \times His-tag⁵⁷—confirm this hypothesis since the aggregation of tau-K18 occurs without an off-pathway process. Future studies will address which of the two sites gives rise to the rod-like protofibrils,⁵⁷ but this result is of significance because it indicates that small changes in sequence composition can affect the structural heterogeneity of fibrillation reactions.

A final interesting observation of this work is the detection of coiled spring-like fibrils (Fig. 3a and b) and annular fibrils (Fig. 9d, inset) under some aggregation conditions. Similar curled/wavy fibril morphology has been observed in a previous study,⁶⁷ for fibrils formed by full-length htau40 and three-repeat domain (K19) constructs. Curled/wavy fibrils were, however, not observed for the tau-K18 construct in that study.⁶⁷ Understanding the mechanical and structural basis for this type of fibril morphology will be an important topic for future study.

Physiological relevance of the existence of a secondary pathway for tau fibrillation

While soluble oligomers and protofibrils are now thought to be the primary cytotoxic species in neurodegeneration,^{3,77} evidence has also been provided for the hypothesis that either fibrils^{78,79} or dynamic species associated with fibrils may also possess toxic potential.⁸⁰ The primary importance of a secondary pathway lies in the fact that such a pathway results in an increase in the fibril load and the heterogeneity of structures that are formed early in aggregation. It is possible that early structures formed on the secondary pathway may cause cytotoxicity, but there is presently no evidence for this hypothesis. Work with fibrils formed by β_2 -microglobulin, α -synuclein, and lysozyme has shown that short fibril fragments possess greater toxic potential than longer fragments.⁸¹ Fragmentation has been shown to be a crucial secondary pathway in the aggregation of β_2 -microglobulin, and it has been postulated that the process provides a mechanism to increase fibril load while simultaneously creating species with enhanced cytotoxicity.^{32,37} With the yeast prion Sup35, it has been demonstrated that the phenotype strength *in vivo* correlates with the brittleness of the fibrils since this promotes prion division.³⁸ It is possible that similar processes operate during tau aggregation *in vivo* during Alzheimer's disease or other tauopathies. Studies with cells and

transgenic mouse models of tauopathies have shown that cell death and cognitive deficits during tau aggregation are uncorrelated with fibril load, and hence, some early species is responsible for toxicity.^{82,83} Future studies will hence address the possibility that fibril heterogeneity as a result of this newly discovered secondary pathway may have toxic roles in disease progression.

Materials and Methods

Protein expression, purification, and characterization

The pET22b plasmid containing the tau-K18 gene (pETtauK18) was made by subcloning from pETtau4RPH, a kind gift from Prof. Takashi Konno.⁸⁴ The tau-K18 protein has 130 residues, spans the four repeats (Q244–E372) of the longest isoform httau40, and has an isoelectric point of 9.71. The protein expression and purification protocol has been described previously.⁵⁷ The purity of the protein was confirmed by SDS-PAGE and electrospray ionization mass spectrometry. The mass of the protein was the expected 13,814 Da when determined using a Synapt G2 HD mass spectrometer (Waters).

Absorbance, fluorescence, and CD spectra were acquired to confirm spectroscopic signatures of the purified protein. The molar extinction coefficient of the protein at 280 nm was determined by a bicinchoninic acid assay (kit from Thermo Scientific) using bovine serum albumin as a standard. A dynamic light scattering experiment was performed to check that the purified protein was monomeric with the expected R_H .^{85,86}

Buffers, solutions, and experimental conditions

All reagents used for experiments were of the highest purity grade available from Sigma, unless otherwise specified. At the start of each experiment, the protein stored in 1× phosphate-buffered saline buffer (pH 7.4) was buffer-exchanged into 25 mM Tris buffer (pH 7) using a PD-10 column (Amersham Biosciences). The protein was then diluted into the aggregation buffer (25 mM Tris buffer, 50 mM NaCl, and 1 mM DTT, pH 7) to the desired concentration and then incubated for 2 h at 37 °C to allow for the reduction of any covalent tau dimers to monomers.⁵⁷ The reaction was then induced by the addition of heparin (molecular mass, 12,000 Da, Himedia Laboratories) of the desired concentration. The final pH remained unchanged, and the aggregation reaction continued to be maintained at 37 °C. The same heating block was used for all the experiments to reduce variability.

Reproducibility in aggregation kinetics

Careful reproducible handling of protein and aggregation reactions was found to be crucial for ensuring the repeatability of the aggregation kinetics. Frozen aliquots of protein were thawed first for 1.5 h on ice and then for 10 min at room temperature before the start of each

experiment. The protein was then spun at 20,000g for 10 min at 4 °C, before buffer exchange was performed using a PD-10 column. Small amounts of NaCl (5–10 mM) were found to cause substantial changes in aggregation kinetics, and hence, the protein was always buffer-exchanged into fresh 25 mM Tris buffer (pH 7). The desired salt concentration was then added from a concentrated stock solution (2 M NaCl). It was important to avoid any error in the determination of protein concentration because of the strong dependence of the aggregation kinetics on protein concentration. Tau-K18 has a low molar extinction coefficient, which could conceivably lead to small errors in protein concentration determination. Hence, the final amplitude of ThT fluorescence during aggregation was used as an additional internal control for protein concentration, as every assay involved the measurement of the fluorescence of 1 μM aggregate sample. Mixing of aggregation reactions before removal of an aliquot for ThT fluorescence or AFM measurement was found to be important in ensuring reproducibility of kinetics, and this was therefore always done at the exact same time point in the exact same manner. Typically, the volume of the aggregating protein solution was 1.0–1.5 ml. At different time points of aggregation, 5- to 50-μl aliquots of the protein sample were withdrawn depending on the protein concentration being studied. Before removing an aliquot, the aggregating solution was mixed three times with a P200 pipette.

ThT fluorescence assay

The ThT assay was done at pH 7 in 25 mM Tris buffer, and a final concentration of 1 μM protein and 10 μM ThT was used. For every reading, a calculated amount of the protein, according to the concentration used in the aggregation experiment, was withdrawn from the sample and added to the ThT assay solution. Measurements were made within 30 s of the addition of the protein to the assay solution, using a Fluoromax-3 spectrofluorimeter (Jobin Yvon) as described earlier.¹⁰

Seeding experiments

For experiments with unsonicated seed, 25 μM tau-K18 was aggregated in the presence of 37.5 μM heparin for three times the t_{50} of ThT fluorescence-monitored kinetics (4 h), and the final fibril suspension was used to seed a fresh aggregation reaction. The fresh aggregation reaction was first induced by the addition of the correct volume of heparin, the reaction mixture was mixed twice, and the relevant volume of mixture was removed and replaced by an equal volume of seed to obtain the % seed desired (v/v).

For experiments with sonicated seed, 25 μM tau-K18 was aggregated in the presence of 37.5 μM heparin for 4 h and the final fibril suspension was then placed on ice and sonicated using a microprobe (Sonics Vibracell). The following settings were used: amplitude, 30%; 5 s on; 4 s off; total time, 2 min. The sonicated seed mixture was then used to seed a fresh aggregation reaction as described above. Across experiments, there was an ~20% variation in the amplitude of ThT fluorescence due to inherent variations in the sonication procedure but fractional change plots normalized for this difference in amplitude

were perfectly reproducible and were hence used to study the difference from unseeded reactions.

Static light scattering assay

The scattering intensity of samples at times corresponding to $3t_{50}$ of ThT fluorescence-monitored kinetics was measured using a Fluoromax-3 spectrofluorimeter (Jobin Yvon). One hundred microliters of samples was withdrawn at the designated times, and the scattering intensity was measured using the following acquisition parameters: excitation and emission wavelength, 800 nm; excitation bandwidth, 1 nm; emission bandwidth, 10 nm; total time, 60 s; averaging time, 2 s. The data plotted correspond to the average of 60 s.

Sedimentation assay

The amount of protein present in the pellet and the supernatant at times corresponding to $3t_{50}$ of ThT fluorescence-monitored kinetics for different protein concentrations was determined using a sedimentation assay coupled to the measurement of Tyr fluorescence at 303 nm as described earlier.⁵⁷ The equilibrium monomer concentration was calculated using a sedimentation assay coupled to ultracentrifugation. Briefly, protein was aggregated for a time corresponding to $3t_{50}$ of ThT fluorescence-monitored kinetics and then the sample was spun at 70,000 rpm for 1 h at 4 °C using the TLA 120.1 rotor in a Beckman Optima™ TL ultracentrifuge. The protein concentration in the supernatant was then measured using Tyr fluorescence at 303 nm.

Atomic force microscopy

AFM samples of fibrils formed at different protein concentrations were made at times $3t_{50}$ of aggregation as determined from ThT fluorescence-monitored kinetics and at specified times. For preparing samples, a 100- μ l neat aliquot of the sample was withdrawn at the designated time, applied onto freshly cleaved mica (Grade V1, SPI supplies), allowed to incubate for 2 min, rinsed with 25 drops of filtered MilliQ water, and then dried under vacuum for 1 h. AFM images were obtained on a PicoPlus AFM instrument (Molecular Imaging Inc.) operating in the non-contact mode using 75-kHz, 2.8- N/m cantilevers with a rounding tip radius of <10 nm (NanoWorld AG). Both small and large scanners (Agilent Technologies) with maximum scan sizes of ~10 and ~100 μ m, respectively, were used for imaging. Image acquisition parameters were as follows: scan speed, 1.0–1.5 lines/s; pixel intensity, 1024 data points/line. The diameters of the fibrils were determined by measuring the Z heights of the structures in the flattened topography images (assuming them to be cylindrical) using the profile option of the program WSxM.⁸⁷

Data analysis and curve fitting

The kinetic curves measured by monitoring ThT fluorescence were fitted to the sigmoidal Eq. (1)

$$S = \frac{S_{\infty}}{1 + e^{-((t-t_{50})/\tau)}} \quad (1)$$

where S_{∞} is the amplitude of signal change, t is the time, t_{50} is the time at which the change in signal is 50%, and τ is a characteristic time constant. The lag time (t_D) was calculated using the formula $t_D = t_{50} - 2\tau$ as described in Ref. 21. This value was found to be the same as that obtained by calculating the time taken to reach 10% (t_{10}) of the reaction.¹⁵

The time, t_f , at which a given fractional extent, f , of aggregation is reached (t_D/t_{10} for a 10% change, or t_{50} for a 50% change) is related to the total protein monomer concentration, c_0 , by Eq. (2).^{12,40,58}

$$\log t_f = \frac{-(i+1)}{2} \log c_0 \quad (2)$$

where i is the number of protein units (monomers) in the oligomeric nucleus, which exists in a highly unfavorable equilibrium with the monomer.

The theory and the equations underlying the analysis of data by the use of the NDP model augmented by a secondary pathway for polymer growth⁴⁰ are briefly summarized below.

The primary pathway is homogeneous nucleation, which is described by equilibrium nucleation theory. Pre-nuclear aggregates, in addition to being in equilibrium with monomers, are also assumed to have concentrations much smaller than either the free monomer concentration or the concentration of polymerized monomers. Hence,

$$\Delta(t) = c_0 - c(t) \quad (3)$$

where $\Delta(t)$ is the concentration of polymerized monomers and $c(t)$ is the concentration of free monomers at time t .

$\Delta(t)$ changes by monomer addition or loss at polymer ends, and this process is assumed to be length independent for long polymers. Hence,

$$\frac{d\Delta}{dt} = (k_+c - k_-)c_p \quad (4)$$

where k_+ and k_- are the rate constants for monomer addition and loss from the polymer ends, respectively, and are identical for all polymer forms. c_p is the concentration of polymers. k_+ and k_- are related by the critical concentration c_s as $k_- = k_+ c_s$

The rate of homogeneous polymer formation can be described as

$$\frac{dc_p}{dt} = k_+cc_i - k_i^*c_{i+1} \quad (5)$$

where the nucleus is of size i and the polymer is of size $(i+1)$ or larger; k_+ and k_i^* are the rate constants for monomer addition and loss from the nucleus, respectively. k_+ is assumed to be the same as the rate constant for monomer addition to the polymer.

Assuming that the nucleus and monomer are in continuous equilibrium with each other (equilibrium nucleation), with the equilibrium defined by the equilibrium constant K_i , the concentration of nuclei, c_i , is equal to $K_i c_i^i$.

Then, since the first term in Eq. (5) dominates over the second term, especially in the initial phase of the reaction, Eq. (5) can be rewritten as

$$\frac{dc_p}{dt} = k_+cc_i = k_+K_i c_i^{i+1} \quad (6)$$

Secondary processes may be of three kinds: fragmentation, branching, or heterogeneous nucleation, with the rate in each case being proportional to the concentration of polymerized monomers ($c_0 - c$). All three processes can be described⁴⁰ by a general parameter Q such that

$$\frac{dc_p}{dt} = k_+ K_i c^{i+1} + Q(c_0 - c) \quad (7)$$

For the initial 10–20% of the data, Eq. (7) can be solved by a linear perturbation approach to yield the solution:

$$\Delta = A[\cosh Bt - 1] \quad (8)$$

where

$$A = \frac{K_i c_0^{i+1}}{(Q_0/k_+) - (i+1)K_i c_0^i} \quad (9)$$

$$B = k_+ \sqrt{(c_0 - c_s)[(Q_0/k_+) - (i+1)K_i c_0^i]} \quad (10)$$

A is a parameter that governs the apparent shape of the progress curve and B is an effective rate constant for nucleation.

A plot of $\log B^2 A / [c_0(c_0 - c_s)]$ versus $\log c_0$ yields the homogeneous nucleus size i by the use of Eq. (11). The value of c_s used in this calculation is 3 μM (see Results).

$$\log \frac{B^2 A}{c_0(c_0 - c_s)} = \log(k_+^2 K_i) + i \log c_0 \quad (11)$$

The parameters A , B , i , c_0 , and c_s (3 μM) are used to determine the value of $k_+ Q_0$ at each value of c_0 , by the use of Eq. (12).

$$k_+ Q_0 = \frac{B^2 + (i+1) \left(\frac{B^2 A}{c_0} \right)}{c_0 - c_s} \quad (12)$$

The nature of the secondary process can then be determined from the dependence of $\log k_+ Q_0$ on $\log c_0$. When the secondary process is fragmentation, such a plot would have a slope of zero; when the secondary process is lateral growth, such a plot would have a slope of unity; and when the secondary process is heterogeneous nucleation, the slope would give the heterogeneous nucleus size.⁴⁰

All fits were performed using the regression wizard of SigmaPlot, which uses the Levenberg–Marquardt algorithm to find the best fit between the data and the equation. Lines that were drawn by inspection are intended to serve as guides for the eye and were drawn using illustration software.

Acknowledgements

We thank members of our laboratory for discussions and comments on the manuscript. We thank Dr. E. B. Lebow, Prof. H. Flyvbjerg, and Prof. M. Rao for discussions and Vishal

Bharadwaj for help in the construction of the pETtauK18 clone. The AFM images were collected at the Central Imaging Facility of the National Centre for Biological Sciences. G.R. is a recipient of the SP Mukherjee Fellowship from the Council of Scientific and Industrial Research, Government of India. J.B.U. is a recipient of the JC Bose National Fellowship from the Government of India. This work was funded by the Tata Institute of Fundamental Research and by the Department of Biotechnology, Government of India.

Supplementary Data

Supplementary data to this article can be found online at [doi:10.1016/j.jmb.2012.01.007](https://doi.org/10.1016/j.jmb.2012.01.007)

References

- Chiti, F. & Dobson, C. M. (2006). Protein misfolding, functional amyloid, and human disease. *Annu. Rev. Biochem.* **75**, 333–366.
- Kumar, S. & Udgaonkar, J. B. (2010). Mechanisms of amyloid fibril formation by proteins. *Curr. Sci.* **98**, 639–656.
- Caughey, B. & Lansbury, P. T. (2003). Protofibrils, pores, fibrils, and neurodegeneration: separating the responsible protein aggregates from the innocent bystanders. *Annu. Rev. Neurosci.* **26**, 267–298.
- Frieden, C. (2007). Protein aggregation processes: in search of the mechanism. *Protein Sci.* **16**, 2334–2344.
- Oosawa, F. & Kasai, M. (1962). A theory of linear and helical aggregations of macromolecules. *J. Mol. Biol.* **4**, 10–21.
- Ferrone, F. (1999). Analysis of protein aggregation kinetics. *Methods Enzymol.* **309**, 256–274.
- Zhao, D. & Moore, J. S. (2003). Nucleation–elongation: a mechanism for cooperative supramolecular polymerization. *Org. Biomol. Chem.* **1**, 3471–3491.
- Roberts, C. J. (2007). Non-native protein aggregation kinetics. *Biotechnol. Bioeng.* **98**, 927–938.
- Kumar, S. & Udgaonkar, J. B. (2009). Structurally distinct amyloid protofibrils form on separate pathways of aggregation of a small protein. *Biochemistry*, **48**, 6441–6449.
- Jain, S. & Udgaonkar, J. B. (2011). Defining the pathway of worm-like amyloid fibril formation by the mouse prion protein by delineation of the productive and unproductive oligomerization reactions. *Biochemistry*, **50**, 1153–1161.
- Toyama, B. H. & Weissman, J. S. (2011). Amyloid structure: conformational diversity and consequences. *Annu. Rev. Biochem.* **80**, 557–585.
- Oosawa, F. & Asakura, S. (1975). *Thermodynamics of the Polymerization of Protein*. Academic Press, London, UK.
- Frieden, C. & Goddette, D. W. (1983). Polymerization of actin and actin-like systems: evaluation of the time course of polymerization in relation to the mechanism. *Biochemistry*, **22**, 5836–5843.
- Tobacman, L. S. & Korn, E. D. (1983). The kinetics of actin nucleation and polymerization. *J. Biol. Chem.* **258**, 3207–3214.

15. Flyvbjerg, H., Jobs, E. & Leibler, S. (1996). Kinetics of self-assembling microtubules: an "inverse problem" in biochemistry. *Proc. Natl Acad. Sci. USA*, **93**, 5975–5979.
16. Harper, J. D. & Lansbury, P. T., Jr (1997). Models of amyloid seeding in Alzheimer's disease and scrapie: mechanistic truths and physiological consequences of the time-dependent solubility of amyloid proteins. *Annu. Rev. Biochem.* **66**, 385–407.
17. Lomakin, A., Chung, D. S., Benedek, G. B., Kirschner, D. A. & Teplow, D. B. (1996). On the nucleation and growth of amyloid beta-protein fibrils: detection of nuclei and quantitation of rate constants. *Proc. Natl Acad. Sci. USA*, **93**, 1125–1129.
18. Wood, S. J., Wypych, J., Steavenson, S., Louis, J. C., Citron, M. & Biere, A. L. (1999). Alpha-synuclein fibrillogenesis is nucleation-dependent. Implications for the pathogenesis of Parkinson's disease. *J. Biol. Chem.* **274**, 19509–19512.
19. Ellisdon, A. M., Pearce, M. C. & Bottomley, S. P. (2007). Mechanisms of ataxin-3 misfolding and fibril formation: kinetic analysis of a disease-associated polyglutamine protein. *J. Mol. Biol.* **368**, 595–605.
20. Chen, S., Ferrone, F. A. & Wetzel, R. (2002). Huntington's disease age-of-onset linked to polyglutamine aggregation nucleation. *Proc. Natl Acad. Sci. USA*, **99**, 11884–11889.
21. Nielsen, L., Khurana, R., Coats, A., Frokjaer, S., Brange, J., Vyas, S. *et al.* (2001). Effect of environmental factors on the kinetics of insulin fibril formation: elucidation of the molecular mechanism. *Biochemistry*, **40**, 6036–6046.
22. Padrick, S. B. & Miranker, A. D. (2002). Islet amyloid: phase partitioning and secondary nucleation are central to the mechanism of fibrillogenesis. *Biochemistry*, **41**, 4694–4703.
23. Frankenfield, K. N., Powers, E. T. & Kelly, J. W. (2005). Influence of the N-terminal domain on the aggregation properties of the prion protein. *Protein Sci.* **14**, 2154–2166.
24. Librizzi, F. & Rischel, C. (2005). The kinetic behavior of insulin fibrillation is determined by heterogeneous nucleation pathways. *Protein Sci.* **14**, 3129–3134.
25. Ferrone, F. A., Hofrichter, J., Sunshine, H. R. & Eaton, W. A. (1980). Kinetic studies on photolysis-induced gelation of sickle cell hemoglobin suggest a new mechanism. *Biophys. J.* **32**, 361–380.
26. Ferrone, F. A., Hofrichter, J. & Eaton, W. A. (1985). Kinetics of sickle hemoglobin polymerization. II. A double nucleation mechanism. *J. Mol. Biol.* **183**, 611–631.
27. Ruschak, A. M. & Miranker, A. D. (2007). Fiber-dependent amyloid formation as catalysis of an existing reaction pathway. *Proc. Natl Acad. Sci. USA*, **104**, 12341–12346.
28. Hall, D. & Edsles, H. (2004). Silent prions lying in wait: a two-hit model of prion/amyloid formation and infection. *J. Mol. Biol.* **336**, 775–786.
29. Collins, S. R., Dougllass, A., Vale, R. D. & Weissman, J. S. (2004). Mechanism of prion propagation: amyloid growth occurs by monomer addition. *PLoS Biol.* **2**, e321.
30. Manno, M., Craparo, E. F., Podesta, A., Bulone, D., Carrotta, R., Martorana, V. *et al.* (2007). Kinetics of different processes in human insulin amyloid formation. *J. Mol. Biol.* **366**, 258–274.
31. Pedersen, J. S., Dikov, D., Flink, J. L., Hjuler, H. A., Christiansen, G. & Otzen, D. E. (2006). The changing face of glucagon fibrillation: structural polymorphism and conformational imprinting. *J. Mol. Biol.* **355**, 501–523.
32. Xue, W. F., Homans, S. W. & Radford, S. E. (2008). Systematic analysis of nucleation-dependent polymerization reveals new insights into the mechanism of amyloid self-assembly. *Proc. Natl Acad. Sci. USA*, **105**, 8926–8931.
33. Andersen, C. B., Otzen, D., Christiansen, G. & Rischel, C. (2007). Glucagon amyloid-like fibril morphology is selected via morphology-dependent growth inhibition. *Biochemistry*, **46**, 7314–7324.
34. Andersen, C. B., Yagi, H., Manno, M., Martorana, V., Ban, T., Christiansen, G. *et al.* (2009). Branching in amyloid fibril growth. *Biophys. J.* **96**, 1529–1536.
35. Patil, S. M., Mehta, A., Jha, S. & Alexandrescu, A. T. (2011). Heterogeneous amylin fibril growth mechanisms imaged by total internal reflection fluorescence microscopy. *Biochemistry*, **50**, 2808–2819.
36. Jansen, R., Dzwolak, W. & Winter, R. (2005). Amyloidogenic self-assembly of insulin aggregates probed by high resolution atomic force microscopy. *Biophys. J.* **88**, 1344–1353.
37. Xue, W. F., Hellewell, A. L., Hewitt, E. W. & Radford, S. E. (2010). Fibril fragmentation in amyloid assembly and cytotoxicity: when size matters. *Prion*, **4**, 20–25.
38. Tanaka, M., Collins, S. R., Toyama, B. H. & Weissman, J. S. (2006). The physical basis of how prion conformations determine strain phenotypes. *Nature*, **442**, 585–589.
39. Knowles, T. P., Waudby, C. A., Devlin, G. L., Cohen, S. I., Aguzzi, A., Vendruscolo, M. *et al.* (2009). An analytical solution to the kinetics of breakable filament assembly. *Science*, **326**, 1533–1537.
40. Bishop, M. F. & Ferrone, F. A. (1984). Kinetics of nucleation-controlled polymerization. A perturbation treatment for use with a secondary pathway. *Biophys. J.* **46**, 631–644.
41. Weingarten, M. D., Lockwood, A. H., Hwo, S. Y. & Kirschner, M. W. (1975). A protein factor essential for microtubule assembly. *Proc. Natl Acad. Sci. USA*, **72**, 1858–1862.
42. Ballatore, C., Lee, V. M. & Trojanowski, J. Q. (2007). Tau-mediated neurodegeneration in Alzheimer's disease and related disorders. *Nat. Rev. Neurosci.* **8**, 663–672.
43. Goedert, M., Spillantini, M. G. & Davies, S. W. (1998). Filamentous nerve cell inclusions in neurodegenerative diseases. *Curr. Opin. Neurobiol.* **8**, 619–632.
44. Garcia, M. L. & Cleveland, D. W. (2001). Going new places using an old MAP: tau, microtubules and human neurodegenerative disease. *Curr. Opin. Cell Biol.* **13**, 41–48.
45. Schweers, O., Schonbrunn-Hanebeck, E., Marx, A. & Mandelkow, E. (1994). Structural studies of tau protein and Alzheimer paired helical filaments show no evidence for beta-structure. *J. Biol. Chem.* **269**, 24290–24297.
46. Mukrasch, M. D., Bibow, S., Korukottu, J., Jeganathan, S., Biernat, J., Griesinger, C. *et al.* (2009). Structural

- polymorphism of 441-residue tau at single residue resolution. *PLoS Biol.* **7**, e34.
47. Goedert, M., Jakes, R., Spillantini, M. G., Hasegawa, M., Smith, M. J. & Crowther, R. A. (1996). Assembly of microtubule-associated protein tau into Alzheimer-like filaments induced by sulphated glycosaminoglycans. *Nature*, **383**, 550–553.
 48. Wilson, D. M. & Binder, L. I. (1997). Free fatty acids stimulate the polymerization of tau and amyloid beta peptides. In vitro evidence for a common effector of pathogenesis in Alzheimer's disease. *Am. J. Pathol.* **150**, 2181–2195.
 49. Chirita, C. N., Necula, M. & Kuret, J. (2003). Anionic micelles and vesicles induce tau fibrillization in vitro. *J. Biol. Chem.* **278**, 25644–25650.
 50. Gustke, N., Trinczek, B., Biernat, J., Mandelkow, E. M. & Mandelkow, E. (1994). Domains of tau protein and interactions with microtubules. *Biochemistry*, **33**, 9511–9522.
 51. Wischik, C. M., Novak, M., Edwards, P. C., Klug, A., Tichelaar, W. & Crowther, R. A. (1988). Structural characterization of the core of the paired helical filament of Alzheimer disease. *Proc. Natl Acad. Sci. USA*. **85**, 4884–4888.
 52. von Bergen, M., Barghorn, S., Muller, S. A., Pickhardt, M., Biernat, J., Mandelkow, E. M. *et al.* (2006). The core of tau-paired helical filaments studied by scanning transmission electron microscopy and limited proteolysis. *Biochemistry*, **45**, 6446–6457.
 53. Friedhoff, P., von Bergen, M., Mandelkow, E. M., Davies, P. & Mandelkow, E. (1998). A nucleated assembly mechanism of Alzheimer paired helical filaments. *Proc. Natl Acad. Sci. USA*. **95**, 15712–15717.
 54. Wille, H., Drewes, G., Biernat, J., Mandelkow, E. M. & Mandelkow, E. (1992). Alzheimer-like paired helical filaments and antiparallel dimers formed from microtubule-associated protein tau in vitro. *J. Cell Biol.* **118**, 573–584.
 55. King, M. E., Ahuja, V., Binder, L. I. & Kuret, J. (1999). Ligand-dependent tau filament formation: implications for Alzheimer's disease progression. *Biochemistry*, **38**, 14851–14859.
 56. Congdon, E. E., Kim, S., Bonchak, J., Songrug, T., Matzavinos, A. & Kuret, J. (2008). Nucleation-dependent tau filament formation: the importance of dimerization and an estimation of elementary rate constants. *J. Biol. Chem.* **283**, 13806–13816.
 57. Ramachandran, G. & Udgaonkar, J. B. (2011). Understanding the kinetic roles of the inducer heparin and of rod-like protofibrils during amyloid fibril formation by Tau protein. *J. Biol. Chem.* **286**, 38948–38959.
 58. Powers, E. T. & Powers, D. L. (2006). The kinetics of nucleated polymerizations at high concentrations: amyloid fibril formation near and above the “super-critical concentration”. *Biophys. J.* **91**, 122–132.
 59. Powers, E. T. & Powers, D. L. (2008). Mechanisms of protein fibril formation: nucleated polymerization with competing off-pathway aggregation. *Biophys. J.* **94**, 379–391.
 60. Wegner, A. & Engel, J. (1975). Kinetics of the cooperative association of actin to actin filaments. *Biophys. Chem.* **3**, 215–225.
 61. Erickson, H. P. & Pantaloni, D. (1981). The role of subunit entropy in cooperative assembly. Nucleation of microtubules and other two-dimensional polymers. *Biophys. J.* **34**, 293–309.
 62. Goldstein, R. F. & Stryer, L. (1986). Cooperative polymerization reactions. Analytical approximations, numerical examples, and experimental strategy. *Biophys. J.* **50**, 583–599.
 63. Wolfe, L. S., Calabrese, M. F., Nath, A., Blaho, D. V., Miranker, A. D. & Xiong, Y. (2010). Protein-induced photophysical changes to the amyloid indicator dye thioflavin T. *Proc. Natl Acad. Sci. USA*. **107**, 16863–16868.
 64. Naiki, H., Higuchi, K., Hosokawa, M. & Takeda, T. (1989). Fluorometric determination of amyloid fibrils in vitro using the fluorescent dye, thioflavin T1. *Anal. Biochem.* **177**, 244–249.
 65. LeVine, H., 3rd (1993). Thioflavine T interaction with synthetic Alzheimer's disease beta-amyloid peptides: detection of amyloid aggregation in solution. *Protein Sci.* **2**, 404–410.
 66. Biancalana, M., Makabe, K., Koide, A. & Koide, S. (2009). Molecular mechanism of thioflavin-T binding to the surface of beta-rich peptide self-assemblies. *J. Mol. Biol.* **385**, 1052–1063.
 67. Wegmann, S., Jung, Y. J., Chinnathambi, S., Mandelkow, E. M., Mandelkow, E. & Muller, D. J. (2010). Human Tau isoforms assemble into ribbon-like fibrils that display polymorphic structure and stability. *J. Biol. Chem.* **285**, 27302–27313.
 68. Fersht, A. (1999). *Structure and Mechanism in Protein Science: A Guide to Enzyme Catalysis and Protein Folding*. W.H. Freeman and Company, New York, NY.
 69. Sibille, N., Sillen, A., Leroy, A., Wieruszeski, J. M., Mulloy, B., Landrieu, I. & Lippens, G. (2006). Structural impact of heparin binding to full-length Tau as studied by NMR spectroscopy. *Biochemistry*, **45**, 12560–12572.
 70. Zhu, H. L., Fernandez, C., Fan, J. B., Shewmaker, F., Chen, J., Minton, A. P. & Liang, Y. (2010). Quantitative characterization of heparin binding to Tau protein: implication for inducer-mediated Tau filament formation. *J. Biol. Chem.* **285**, 3592–3599.
 71. Chirita, C. N., Congdon, E. E., Yin, H. & Kuret, J. (2005). Triggers of full-length tau aggregation: a role for partially folded intermediates. *Biochemistry*, **44**, 5862–5872.
 72. Kuret, J., Chirita, C. N., Congdon, E. E., Kannanayakal, T., Li, G., Necula, M. *et al.* (2005). Pathways of tau fibrillization. *Biochim. Biophys. Acta*, **1739**, 167–178.
 73. Briehl, R. W., Mann, E. S. & Josephs, R. (1990). Length distributions of hemoglobin S fibers. *J. Mol. Biol.* **211**, 693–698.
 74. Necula, M. & Kuret, J. (2004). A static laser light scattering assay for surfactant-induced tau fibrillization. *Anal. Biochem.* **333**, 205–215.
 75. Wilson, D. M. & Binder, L. I. (1995). Polymerization of microtubule-associated protein tau under near-physiological conditions. *J. Biol. Chem.* **270**, 24306–24314.
 76. Chirita, C. N. & Kuret, J. (2004). Evidence for an intermediate in tau filament formation. *Biochemistry*, **43**, 1704–1714.
 77. Kaye, R., Head, E., Thompson, J. L., McIntire, T. M., Milton, S. C., Cotman, C. W. & Glabe, C. G. (2003). Common structure of soluble amyloid oligomers

- implies common mechanism of pathogenesis. *Science*, **300**, 486–489.
78. Gharibyan, A. L., Zamotin, V., Yanamandra, K., Moskaleva, O. S., Margulis, B. A., Kostanyan, I. A. & Morozova-Roche, L. A. (2007). Lysozyme amyloid oligomers and fibrils induce cellular death via different apoptotic/necrotic pathways. *J. Mol. Biol.* **365**, 1337–1349.
 79. Pieri, L., Bucciantini, M., Nosi, D., Formigli, L., Savistchenko, J., Melki, R. & Stefani, M. (2006). The yeast prion Ure2p native-like assemblies are toxic to mammalian cells regardless of their aggregation state. *J. Biol. Chem.* **281**, 15337–15344.
 80. Carulla, N., Caddy, G. L., Hall, D. R., Zurdo, J., Gairi, M., Feliz, M. *et al.* (2005). Molecular recycling within amyloid fibrils. *Nature*, **436**, 554–558.
 81. Xue, W. F., Hellewell, A. L., Gosal, W. S., Homans, S. W., Hewitt, E. W. & Radford, S. E. (2009). Fibril fragmentation enhances amyloid cytotoxicity. *J. Biol. Chem.* **284**, 34272–34282.
 82. Andorfer, C., Acker, C. M., Kress, Y., Hof, P. R., Duff, K. & Davies, P. (2005). Cell-cycle reentry and cell death in transgenic mice expressing nonmutant human tau isoforms. *J. Neurosci.* **25**, 5446–5454.
 83. Santacruz, K., Lewis, J., Spire, T., Paulson, J., Kotilinek, L., Ingelsson, M. *et al.* (2005). Tau suppression in a neurodegenerative mouse model improves memory function. *Science*, **309**, 476–481.
 84. Konno, T., Oiki, S., Hasegawa, K. & Naiki, H. (2004). Anionic contribution for fibrous maturation of protofibrillar assemblies of the human tau repeat domain in a fluoroalcohol solution. *Biochemistry*, **43**, 13613–13620.
 85. Yao, T. M., Tomoo, K., Ishida, T., Hasegawa, H., Sasaki, M. & Taniguchi, T. (2003). Aggregation analysis of the microtubule binding domain in tau protein by spectroscopic methods. *J. Biochem.* **134**, 91–99.
 86. Mylonas, E., Hascher, A., Bernado, P., Blackledge, M., Mandelkow, E. & Svergun, D. I. (2008). Domain conformation of tau protein studied by solution small-angle X-ray scattering. *Biochemistry*, **47**, 10345–10353.
 87. Horcas, I., Fernandez, R., Gomez-Rodriguez, J. M., Colchero, J., Gomez-Herrero, J. & Baro, A. M. (2007). WSXM: a software for scanning probe microscopy and a tool for nanotechnology. *Rev. Sci. Instrum.* **78**, 013705.